Modeling Freckle Formation in Three Dimensions during Solidification of Multicomponent Alloys

S.D. FELICELLI, D.R. POIRIER, and J.C. HEINRICH

The formation of macrosegregation defects known as ''freckles'' was simulated using a three-dimensional finite element model that calculates the thermosolutal convection and macrosegregation during the dendritic solidification of multicomponent alloys. A recently introduced algorithm was used to calculate the complicated solidification path of alloys of many components, which can accommodate liquidus temperatures that are general functions of liquid concentrations. The calculations are started from an all-liquid state, and the growth of the mushy zone is followed in time. Simulations of a Ni-Al-Ta-W alloy were performed on a rectangular cylinder until complete solidification. The results reveal details of the formation of freckles not previously observed in two-dimensional simulations. Liquid plumes in the form of chimney convection emanate from channels within the mushy zone, with similar qualitative features previously observed in transparent systems. Associated with the formation of channels, there is a complex three-dimensional flow produced by the interaction of the different solutal buoyancies of the alloy solutes. Regions of enhanced solid growth develop around the channel mouths, which are visualized as volcanoes on top of the mushy zone. The prediction of volcanoes differs from our previous calculations with multicomponent alloys in two dimensions, in which the volcanoes were not nearly as apparent. These and other features of freckle formation phenomena are illustrated.

I. INTRODUCTION

MATHEMATICAL modeling of alloy solidification with a ''mushy zone'' (solid plus liquid region) involves the simultaneous solution to the equations of momentum, energy, and mass transport. Analysis of transport phenomena during dendritic solidification is a prerequisite for understanding macrosegregation in cast products. One of the most severe forms of macrosegregation is manifested as defects known as ''freckles,'' which develop in directional solidification (DS) processes effected vertically. Vertical DS provides an effective means of controlling the grain shape, producing a columnar microstructure with all the grain boundaries parallel to the longitudinal direction of the casting. In conjunction with a grain selector or a preoriented seed at the bottom of the casting, directional solidification is used to make entire castings that are dendritic single crystals.[1]

Unfortunately, freckles can form during DS that are sufficient cause to scrap these expensive castings. Freckles are observed as long and narrow trails, aligned roughly parallel to the direction of gravity, enriched in the normally segregating elements and depleted of the inversely segregating elements. Several experimental works with nonmetallic transparent systems have provided conclusive evidence that freckles are a direct consequence of upward flowing liquid plumes that emanate from channels within the mushy zone (*e.g.*, Copley *et al.*[2] and Chen and Chen[3]). Observation of freckles in quenched Pb-Sn alloys (Tewari *et al.*[4] and Sarazin and Hellawell[5]) and Ni-base superalloys (Giamei and Kear[6]) suggests that freckles in metallic alloys also form by the same mechanism. The channels that form in the mushy zone during solidification and that lead to freckling in the solidified casting are a manifestation of localized remelting produced by thermosolutal convection.

Because of the technological importance of the DS process, there have been many works on simulating transport phenomena in directionally solidified castings using the full set of conservation equations. In 1991, the authors simulated channels and freckles in directionally solidified Pb-Sn alloys,[7] and several numerical works dealing with binary alloys followed.[8,9,10] The prediction of macrosegregation in alloys with two or more solutes dates back to 1970, when Fujii *et al.*[11] considered a simplified model of convection in the mushy zone. Models for multicomponent alloys that include thermosolutal convection, both in the liquid and mushy zone, started appearing in 1995[12–15] and will probably be widely applied in the near future due to the fact that most alloys of practical interest comprise many elements. The modeling of multicomponent alloys requires different algorithmic strategies than the ones used for binary alloys. In particular, knowledge of the temperature in the mushy zone does not automatically provide concentration in the interdendritic liquid, a feature on which most binary models rely, making it more difficult to calculate the solidification path. A method of following the complete solidification path in ternary alloys, including the primary phase, binary eutectic, ternary eutectic, and peritectic reaction can be found in Krane and Incropera.[16]

A simplification that has been adopted by practically all freckle-predicting models so far is to assume two-dimensional transport phenomena. Because freckles are very narrow (about 1 mm in diameter), a fine mesh resolution is needed to properly simulate their formation, as well as the associated segregation. This fact, jointly with the high com-

S.D. FELICELLI, Research Scientist, is with Centro Atómic Bariloche, 8400 S.C. de Bariloche, Argentina. D.R. POIRIER, Professor, Department of Materials Science and Engineering, and J.C. HEINRICH, Professor, Department of Aerospace and Mechanical Engineering, are with the University of Arizona, Tucson, AZ 85721.

Manuscript submitted August 1, 1997.

putational cost of solving tridimensional convection, has deterred exploration in this area. Although much has been learned from two-dimensional models, channel formation is obviously a tridimensional phenomenon, where liquid metal feeds a channel from all directions and dictates the formation and growth of the channel.

To the authors' knowledge, there is no published work on tridimensional simulations of freckles in multicomponent alloys. As to binary alloys, Neilson and Incropera[17] solved the unidirectional solidification of an aqueous ammonium chloride solution in a cylindrical domain. Because their calculation was computationally too expensive to be used to solve the entire cylinder, they considered a 60 deg, sector with cyclic boundary conditions. In spite of this simplification, their results reproduced typical features of channels in NH_2Cl-H_2O systems. However, by computing a rather large domain, the coarseness of the mesh and the associated loss of resolution meant that some details of the channels were lost. Recently, Felicelli *et al.*[18] developed a fully three-dimensional finite element model to simulate the formation of freckles in a Pb-Sn alloy solidifying in cylinders of square and circular cross sections.

In the present work, we have performed tridimensional simulations of a quaternary Ni-Al-Ta-W alloy solidifying vertically in a mold of rectangular cross section. The entire casting surrounded by solid walls is considered, but the dimensions of the castings are kept small so that a fine mesh resolution can be used. The objective is to show full details of the formation of channels and volcanoes in multicomponent alloys that have not yet been seen in existing two-dimensional calculations, jointly with the convection and solute transport associated with them.

II. MATHEMATICAL MODEL

The model for the solidification of multicomponent alloys is an extension of the model for binary alloys developed by the authors[9] and was recently introduced in the context of two-dimensional calculations.[13,14,19] A set of equations of conservation of mass, energy, and solute concentration is solved in conjunction with the momentum equations. The mushy zone is treated as a porous medium of variable porosity (*i.e.*, volume fraction of liquid). The fraction of liquid varies from zero (all-solid region) to one (all-liquid region) in such a way that, when the volume fraction of liquid is zero, no fluid motion is possible and the system reduces to the energy equation. When the volume fraction of the liquid is one, the equations automatically become the Navier–Stokes and transport equations for an all-liquid region. This type of model, known as a continuum model, has been used extensively by us and others in simulations of solidification. The main assumptions used in the development of the governing equations are as follows.

(1) Only solid and liquid phases may be present. No pores form.
(2) The liquid is Newtonian and incompressible, and the flow is laminar.
(3) The solid and liquid phases have equal and constant physical properties.
(4) There is no solute diffusion in the solid phase.
(5) The Boussinesq approximation is made, by which the density is constant except in the body force term of the momentum equations.
(6) The solid is stationary.

With the previous simplifications, the governing equations become as follows.

Continuity:

$$\nabla \cdot \boldsymbol{u} = 0 \qquad [1]$$

Momentum:

$$\phi \frac{\partial}{\partial t}\left(\frac{\boldsymbol{u}}{\phi}\right) + \frac{\mu}{\rho_0}\phi \mathbf{K}^{-1}\boldsymbol{u} - \frac{\mu}{\rho_0}\nabla^2 \boldsymbol{u} + \frac{\phi}{\rho_0}\nabla p = -\boldsymbol{u}\cdot\nabla\left(\frac{\boldsymbol{u}}{\phi}\right) + \frac{\rho}{\rho_0}\phi \boldsymbol{g} \qquad [2]$$

$$\rho = \rho_0\left[1 + \beta_T\left(T - T_R\right) + \sum_{j=1}^{N}\beta_C^j\left(C_l^j - C_R^j\right)\right] \qquad [3]$$

$$\beta_T = \frac{1}{\rho_0}\frac{\partial \rho}{\partial T}; \qquad \beta_C^j = \frac{1}{\rho_0}\frac{\partial \rho}{\partial C_l^j}$$

Energy:

$$\frac{\partial T}{\partial t} - \alpha \nabla^2 T = -\frac{L}{c}\frac{\partial \phi}{\partial t} - \boldsymbol{u}\cdot\nabla T \qquad [4]$$

Conservation of solute components:

$$\frac{\partial \overline{C}^j}{\partial t} = \nabla\cdot\left(D^j\phi\,\nabla\, C_l^j\right) - \boldsymbol{u}\cdot\nabla C_l^j \qquad [5]$$

In these equations, ∇ is the gradient operator, $\boldsymbol{u}$ is the velocity, ϕ is the volume fraction of liquid, t is time, μ is the viscosity, $\mathbf{K}$ is the permeability, p is the pressure, $\boldsymbol{g}$ is gravity, T is temperature, α is the thermal diffusivity, L is the latent heat, c is the specific heat, D^j is the diffusivity of solute j in the liquid, and T_R and C_R^j are reference values for which $\rho = \rho_0$. The permeability is expressed in the principal directions in terms of the volume fraction of liquid and the primary dendrite arm spacing.[7]

The total or mixture concentration, $\overline{C}^j$, and the concentrations in the liquid and solid phases for each solute component are related by

$$\overline{C}^j = \phi C_l^j + \left(1 - \phi\right)\overline{C}_S^j \qquad [6]$$

and, because no diffusion in the solid is assumed, $\overline{C}_S$ is given by

$$\overline{C}_S^j = \frac{1}{1-\phi}\int_{\phi}^{1} k^j\, C_l^j\, d\phi \qquad [7]$$

where k^j is the equilibrium partition ratio of solute j. Finally, the model assumes that the liquidus temperature in the mushy zone is a function of the local composition (no undercooling is allowed). A complete description of the algorithm is given in Reference 19.

The equations described previously were discretized and integrated in time using a finite element method based on the bilinear Lagrangian isoparametric element. A Petrov–Galerkin technique is used to treat the convective terms of the transport equations. The momentum equations were solved with the Galerkin/least-squares method, using equal-order trilinear interpolation for both velocity and pressure, as described by Hughes *et al.*[20] A conjugate gradient al-

Table I. Thermodynamic and Transport Properties Used in the Calculations[21]

Reference concentrations (wt pct): $C_R^{Al} = 6$, $C_R^{Ta} = 6$, $C_R^{W} = 5$

Reference temperature (K): $T_R = 1697$

Eutectic temperature (K): $T_E = 1642$

Equilibrium partition ratios: $k^{Al} = 0.96$

$k^{Ta} = 0.5655 + 0.0183\ C_l^{Ta}$

$k^{W} = 1.67$

Liquidus temperature (K):

$$T_L = 1728 + 2.23354\ C_l^{Al} - 0.0584719\ C_l^{Ta} + 2.4\ C_l^{W} - 2.45034\ (C_l^{Al})^{1.5} - 0.384719\ (C_l^{Ta})^{1.5} - 0.96448\ (C_l^{Al}\ C_l^{Ta})^{0.75}$$

(C_l^{Al}, C_l^{Ta}, and C_l^{W} in wt pct)

Thermal expansion coefficient (K^{-1}): $\beta_T = -1.386 \times 10^{-4}$

Solutal expansion coefficients (wt pct^{-1}):

$$\beta_C^{Al} = -2.457 \times 10^{-2}, \qquad \beta_C^{Ta} = 4.617 \times 10^{-3}, \qquad \beta_C^{W} = 5.241 \times 10^{-3}$$

Viscosity (N s m^{-2}): $\mu = 4.635 \times 10^{-3}$

Specific heat (J kg^{-1} K^{-1}): $c = 700$

Latent heat (J kg^{-1}): $L = 2.95 \times 10^{5}$

Thermal conductivity (W K^{-1} m^{-1}): $\kappa = 30$

Density (kg m^{-3}): $\rho_0 = 7194$

Solute diffusivity in liquid (m^2 s^{-1}): $D = 5 \times 10^{-9}$

Primary dendrite arm spacing (μm): $d_1 = 400$

Permeability (m^2):

$$K_x = K_y = \begin{cases} 1.09 \times 10^{-3}\ \phi^{3.32}\ d_1^2 & \phi < 0.65 \\ 4.04 \times 10^{-6} \left(\dfrac{\phi}{1-\phi}\right)^{6.7336} d_1^2 & 0.65 \le \phi < 0.75 \\ \left[-6.49 \times 10^{-2} + 5.43 \times 10^{-2} \left(\dfrac{\phi}{1-\phi}\right)^{0.25}\right] d_1^2 & 0.75 \le \phi < 1 \end{cases}$$

$$K_z = \begin{cases} 3.75 \times 10^{-4}\ \phi^2\ d_1^2 & \phi < 0.65 \\ 2.05 \times 10^{-7} \left(\dfrac{\phi}{1-\phi}\right)^{10.739} d_1^2 & 0.65 \le \phi < 0.75 \\ 0.074 \left[\log (1-\phi)^{-1} - 1.49 + 2(1-\phi) - 0.5(1-\phi)^2\right] d_1^2 & 0.75 \le \phi < 1 \end{cases}$$

gorithm with diagonal preconditioning and sparse format storage was employed in the solution of the algebraic equations.

III. RESULTS

A quaternary Ni-base alloy was directionally solidified by simulation in a rectangular cylinder of dimensions 10 mm in the x direction, 20 mm in the y direction, and 30 mm in the z direction (height). This domain was discretized with a finite element mesh of trilinear ''brick'' elements, consisting of 20 elements in the x direction, 40 elements in the y direction, and 30 elements in the z direction. This gives a total of 24,000 elements and 26,691 nodes. With four unknowns per node (three velocities and pressure), the dimension of the matrix resulting from the discretization of the momentum equations exceeds 100,000 unknowns. It is evident that, in order to keep the calculations within reasonable limits of computational cost, we must restrict the number of nodes used in the discretization. On the other hand, from experience in the simulation of freckles, we know that the mesh size must be 1 mm or less in order to properly resolve the formation and evolution of channels. For this reason, the size of the computational domain must be relatively small. Calculations in larger domains with coarse meshes are possible too, but the occurrence of channels could be missed and the macrosegregation computed in this way could exhibit a large error.

The composition of the alloy used in the calculations was 6 wt pct Al, 6 wt pct Ta, 5 wt pct W, and the balance Ni. Table I lists the thermodynamic and transport properties of this alloy, which were extracted from a recent work about the sensitivity of macrosegregation to variations of the physical properties.[21]

The simulation starts with an all-liquid alloy of nominal composition in a stable vertical gradient such that the bottom temperature is slightly above that of the liquidus temperature of the nominal alloy. At time $t = 0$, a constant cooling rate, r, is applied at the base of the casting, and a constant temperature gradient, G, is imposed at the top. The

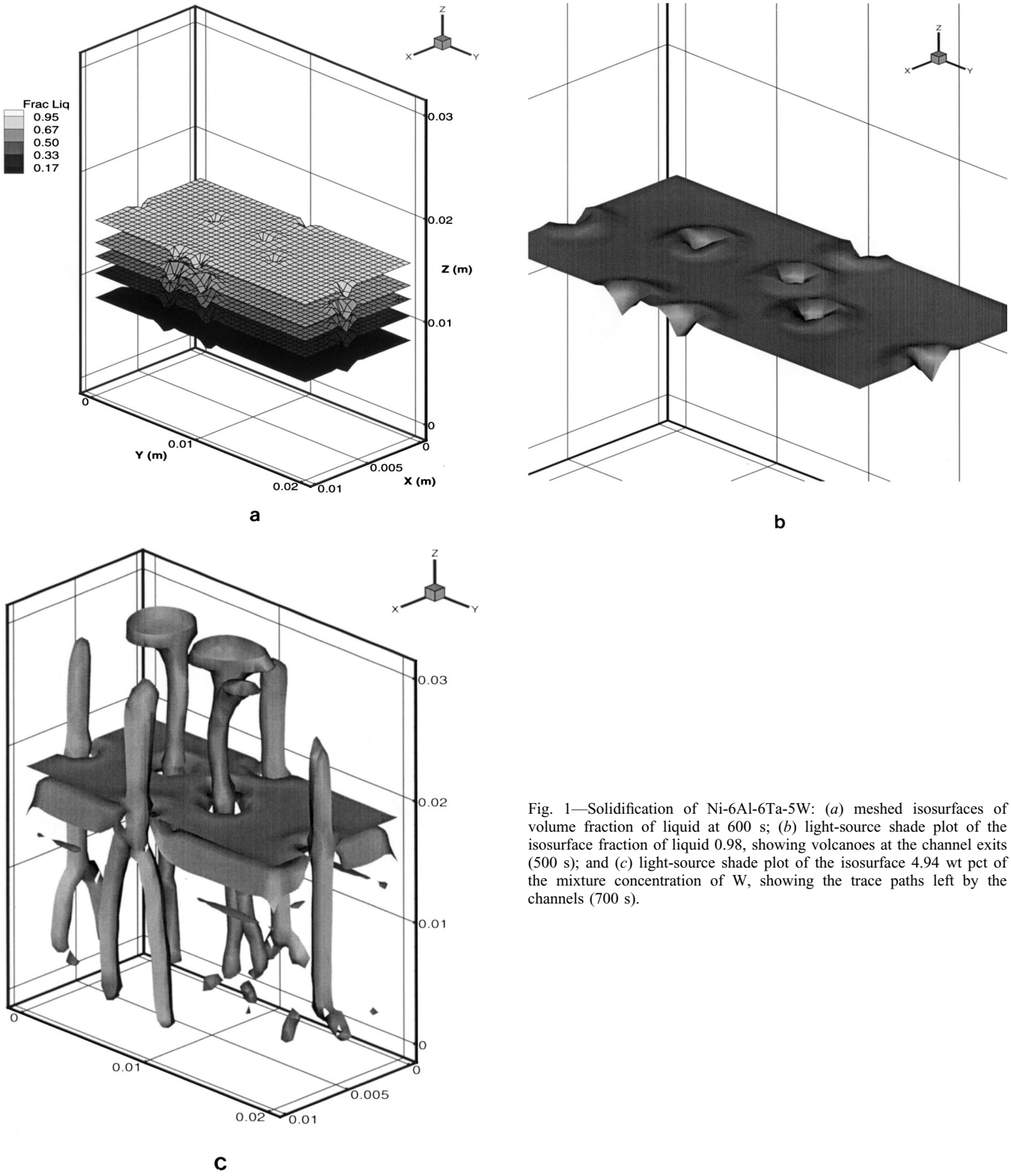

Fig. 1—Solidification of Ni-6Al-6Ta-5W: (*a*) meshed isosurfaces of volume fraction of liquid at 600 s; (*b*) light-source shade plot of the isosurface fraction of liquid 0.98, showing volcanoes at the channel exits (500 s); and (*c*) light-source shade plot of the isosurface 4.94 wt pct of the mixture concentration of W, showing the trace paths left by the channels (700 s).

lateral surfaces are left insulated. It is assumed that the alloy fills the domain completely and is enclosed by solid walls; therefore, no-slip boundary conditions are applied on all surfaces. Initially, the concentration field of each alloy element is perturbed with a random number generator with a maximum perturbation of 0.5 wt pct in order to excite the convection, allowing the system to evolve undisturbed thereafter. The applied cooling rate at the base of the casting was $r = 0.1$ K/s, and the temperature gradient was $G = 2000$ K/m. With these cooling conditions, the solidification proceeded with an average growth rate of 2.6×10^{-5} m/s.

The ability of the fine mesh resolution to capture details of the formation of freckles can be appreciated in the figures that follow. Figure 1(a) shows isosurfaces of the fraction of liquid after 600 seconds of solidification. Five

isosurfaces are plotted, each one with a different gray shade denoting a particular value of fraction of liquid along the surface. The mushy zone extends from $z = 5$ mm to $z = 16$ mm. Below 5 mm, the alloy is all solid, and above 16 mm, it is all liquid. The isosurfaces are meshed to better visualize the irregularities on them. It is observed that several channels have formed: five channels on the mold surface and three internal channels. The channels are not completely open; *i.e.*, the fraction of liquid is less than one along them, but it is significantly higher than the fraction of liquid of the region surrounding the channels, allowing more liquid flow and consequently stronger segregation. Most of the flow to a channel enters it very near the liquidus, as in the experimental results of Hellawell *et al.*[22] and also predicted by Krane and Incropera.[23] This is because of the difficulty in entraining liquid through the much less permeable mushy zone below the liquidus. The predicted results are probably grid dependent, in that, perhaps with more than two or three grid points across a channel, it would be completely open. Enhanced solid growth is found at the mouths of the channels on top of the mushy zone. This can be clearly visualized in Figure 1(b), which is a light-source shaded plot of the isosurface $\phi = 0.95$. The volcano-shaped regions surrounding the channel exits look similar to those observed in experiments with transparent aqueous ammonium chloride solutions.[2,3,22]

A complete view of the structure of freckles and plumes is seen in Figure 1(c), which shows a light-source shaded plot of the isosurface corresponding to a value of 4.94 wt pct in the mixture concentration of W at 700 seconds. The ''pipe'' structures correspond to the positions of plumes and channels, which are freckles below $z = 6$ mm, where the alloy is already solidified. Inside the pipes, the concentration of tungsten is less than 4.94 wt pct. The horizontal surface with flaps is also part of the isosurface and is situated at $z = 18$ mm, just above the top of the mushy zone. Notice the wandering and merging of channels in both the interior and on the mold walls, a feature that has been observed in cast Ni-base superalloys.[6] The mushroom shape of some of the plumes at the top is due to their impingement on the top wall of the container. The composition everywhere is roughly uniform and approximately equal to the initial composition, except in the lower parts of the channels and the freckle trails, where the mixture concentration of Ta has increased up to 6.5 wt pct. Similar plots result for the concentrations of Al and W, because all the solutes are convected with the same velocity field in a situation in which the macrosegregation is dominated by convection. Tungsten, however, is depleted in the channels and freckles due to its partition ratio being greater than one.

The preference of channels to form along the mold walls was also observed in two-dimensional calculations.[13,14] Although one might conjecture that this is due to the no-slip boundary condition, there is no apparent preference for channels to form along the edges of the mold. This is probably because of the smaller feeding area surrounding a channel in a corner. A feature that differs from our previous calculations with multicomponent alloys in two dimensions is the much more evident formation of volcanoes at the mouths of the channels, denoting that the three-dimensional feeding of liquid is important to predict these shapes. Also, it appears that our fine grid is needed to predict the volcanoes at the channel openings. Neilson and Incropera[17] used a coarser grid than we used and were able to predict vertical channels but not the volcanoes.

The sequence shown in Figures 2(a) through (d) illustrates the dynamic behavior of channels during solidification. The mixture concentration of W is plotted for the completely solidified alloy. The same gray scale is used for all the figures. Successive horizontal cross sections, from the bottom up, show the changing positions and number of freckles produced by the wandering and merging of channels during solidification.

The convective instability that leads to freckling in this alloy under certain cooling conditions is caused by the elements Al and W. Aluminum partitions to the interdendritic liquid in the mushy zone; hence, its concentration increases with the distance below the leading part of the mushy zone, making the liquid less dense from below. This, of course, tends to make the liquid convectively unstable. Tantalum also partitions to the interdendritic liquid, but it makes the liquid more dense from below. Hence, it tends to make the liquid stable with respect to convection. Tungsten, like tantalum, increases the density of the interdendritic liquid, but it partitions to the solid so that it tends to make the liquid unstable with respect to convection. Hence, both aluminum and tungsten are solutes that enhance convection and make the alloy more prone to the formation of freckles. Since aluminum partitions weakly and tungsten partitions strongly, tungsten is the more serious culprit in forming freckles.

In Figure 3, we show details of the velocity field associated with the plumes. Figure 3 is a full view of the top of the mushy zone (isosurface $\phi = 0.96$) to which we superimposed the velocity vectors of the flow emerging from the channels. In order to better visualize the velocity field, the velocity vectors were plotted only in regions where the mixture concentration of tungsten is less than 4.95, *i.e.*, regions that correspond approximately to the pipe shapes shown in Figure 1(c). In these regions, the flow is upward due to solutal buoyancy. The speed of the liquid emerging from the three channels is greater than the speed emerging from the channels at the vertical walls, which is retarded by the viscous forces at the walls. The plumes coming out of the internal channels wander, while the ones on the walls are relatively straight. Notice also the impingement of the internal plumes on the top wall.

A close-up view of the fluid flow in the vicinity of a volcano located near the (0,0,z) edge of the casting is shown in Figure 4. To enhance visualization, a circular cylinder surrounding the volcano was selected as the plot zone for velocity vectors. The Ta-enriched liquid emerges upward from the channel, while more dilute liquid feeds back into the walls of the volcano, contributing to its formation.

The simulations presented in this work were done in a Silicon Graphics Power Challenge supercomputer. With the present version of the code, the simulation shown in Figure 1(a) (*i.e.*, 10 minutes of solidification) demands 95 MB of memory and 42 hours of CPU time in one processor of the Power Challenge. More than 80 pct of the computer time is spent in the construction of the element matrices and solution of the algebraic equations, in particular, the momentum equations. By employing an element-by-element technique, these operations can be efficiently parallelized

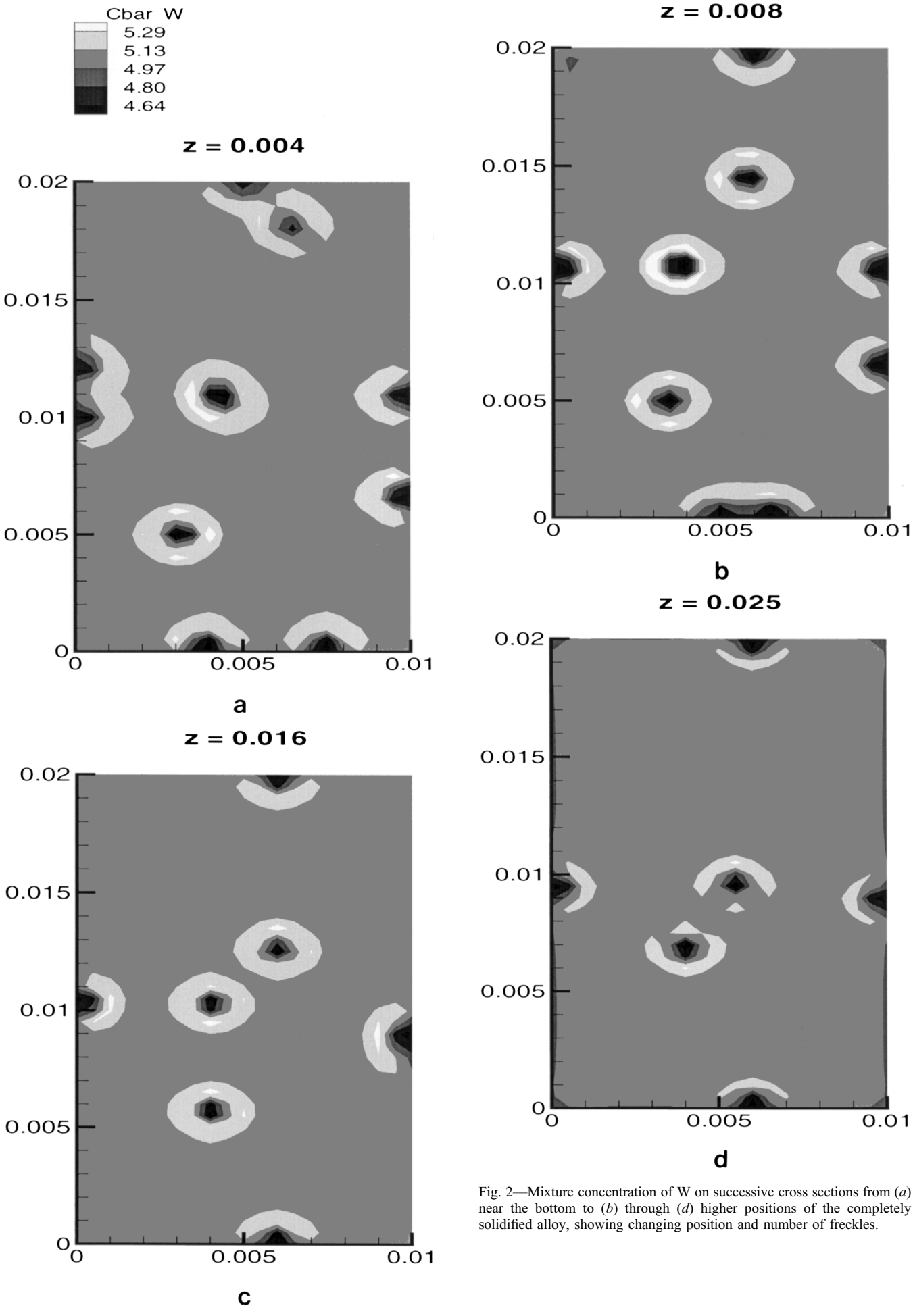

Fig. 2—Mixture concentration of W on successive cross sections from (*a*) near the bottom to (*b*) through (*d*) higher positions of the completely solidified alloy, showing changing position and number of freckles.

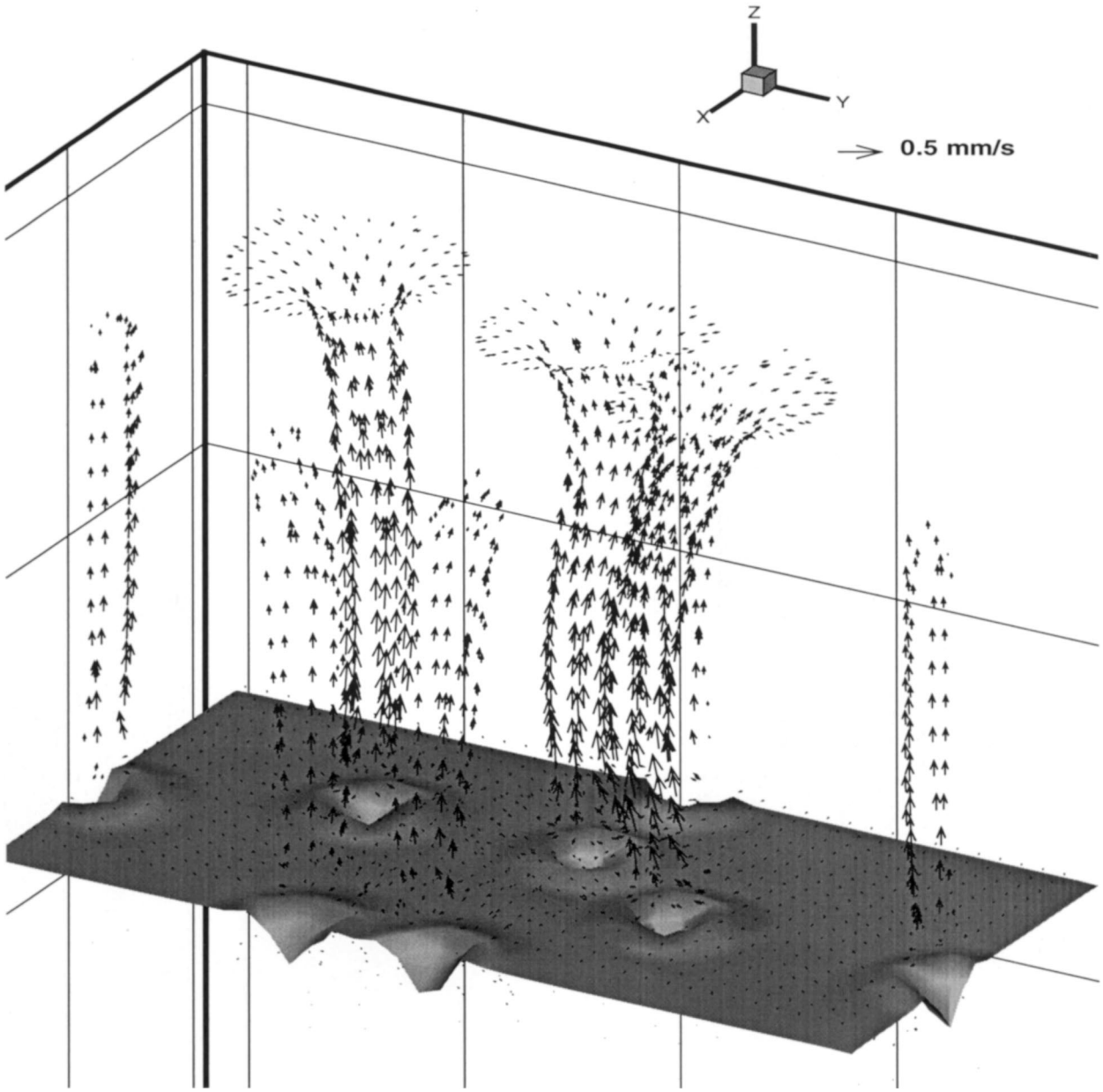

Fig. 3—Upward flow emerging from channels at 500 s. The top of the mushy zone is indicated by the isosurface fraction of liquid of 0.96.

and the memory requirements reduced. Hence, considerably larger problems could be solved in multiprocessor machines.

IV. CONCLUSIONS

Using an algorithm for calculating the solidification of a multicomponent alloy, the three-dimensional characteristics of channels leading to freckle defects were predicted. Simulations of directional solidification of a quaternary nickel-base alloy were performed on a rectangular cylinder. The simulations revealed regions of enhanced solid growth that developed around the mouths of the channels, which appear as volcanoes on top of the mushy zone. Predicting volcanoes was not realized in our previous two-dimensional calculations.[14] Associated with these channels, three-dimensional flows produced by the interaction of different solutal buoyancies of the alloy elements were seen. Emanating from each volcano is a plume. Most of the flow to the upward rising plume is from the overlying liquid, which enters the channel very near its mouth. This is because of the difficulty in entraining liquid through the much less permeable mushy zone below the liquidus.

ACKNOWLEDGMENTS

This work was supported by the Advanced Research Project Agency under the Micromodeling Program of the Investment Casting Cooperative Arrangement under Contract No. MDA972-93-2-0001 and by the National Aeronautics and Space Administration, Microgravity Division, under Contract No. NCC8-96. The authors appreciate the collaboration of P.K. Sung, Department of Materials Science and Engineering, for collecting and analyzing the physical prop-

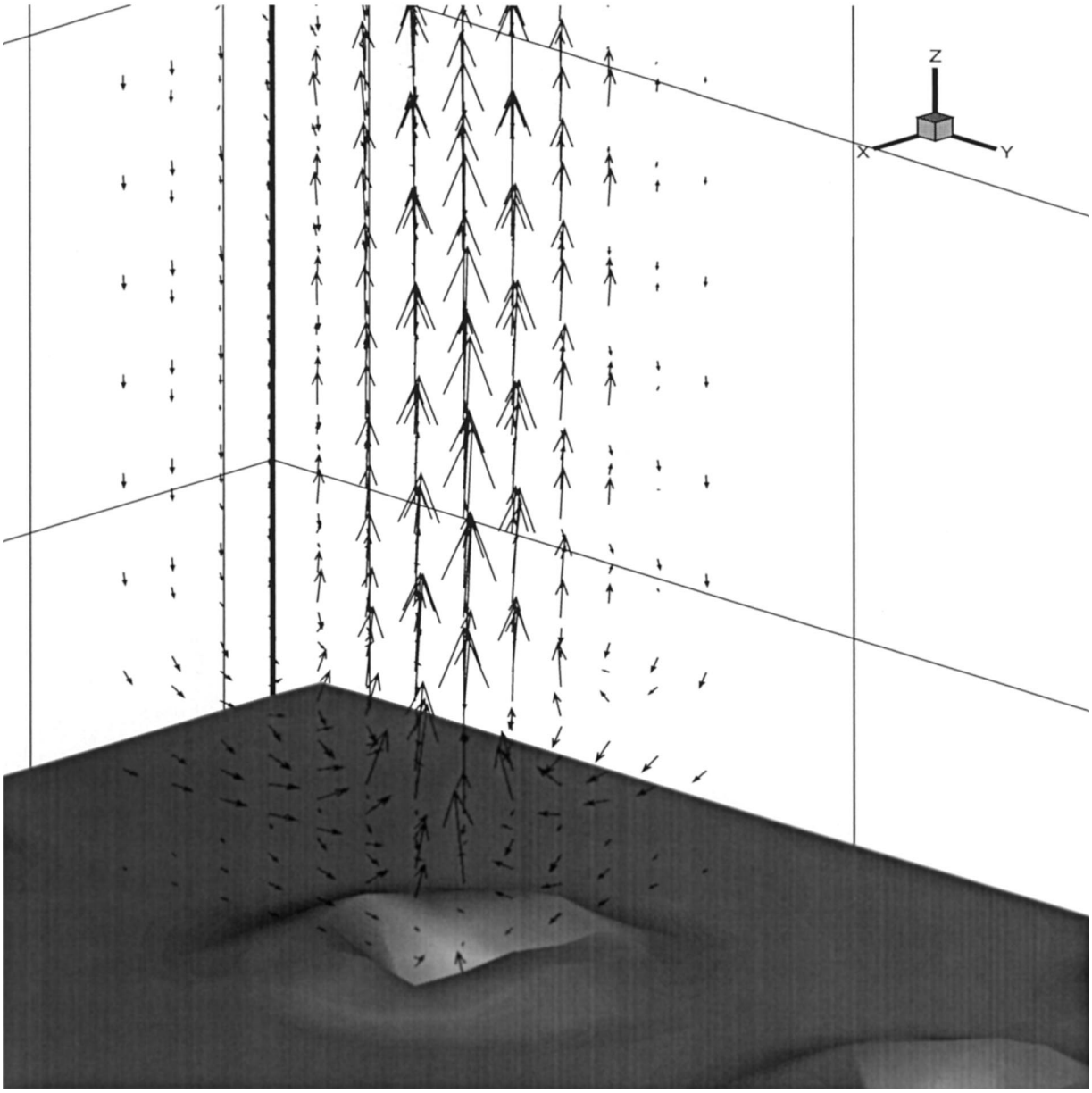

Fig. 4—Details of the velocity field at the mouth of a channel (volcano).

erties used in the simulations. The provision of financial support to SDF by Consejo Nacional de Investigaciones Científicas y Técnicas (CONICET, Argentina) and by Comisión Nacional de Energía Atómica (CNEA, Argentina) is gratefully acknowledged.

REFERENCES

1. P.R. Beeley: in *Investment Casting*, P.R. Beeley and R.F. Smart, eds., The Institute of Materials, London, 1995, pp. 374-91.
2. S.M. Copley, A.F. Giamei, S.M. Johnson, and M.F. Hornbecker: *Metall. Trans.*, 1970, vol. 1, pp. 2193-2204.
3. F. Chen and C.F. Chen: *J. Fluid Mech.*, 1991, vol. 227, pp. 567-86.
4. S.N. Tewari, R. Shah, and M.A. Chopra: *Metall. Trans. A*, 1993, vol. 24A, pp. 1661-69.
5. J.R. Sarazin and A. Hellawell: *Metall. Trans. A*, 1988, vol. 19A, pp. 1861-71.
6. A.F. Giamei and B.H. Kear: *Metall. Trans.*, 1970, vol. 1, pp. 2185-92.
7. S.D. Felicelli, J.C. Heinrich, and D.R. Poirier: *Metall. Trans. B*, 1991, vol. 22B, pp. 847-59.
8. J.C. Heinrich, S.D. Felicelli, and D.R. Poirier: *Comp. Meth. Appl. Mech. Eng.*, 1991, vol. 89, pp. 435-61.
9. S.D. Felicelli, J.C. Heinrich, and D.R. Poirier: *Num. Heat Transfer B*, 1993, vol. 23, pp. 461-81.
10. D.G. Neilson and F.P. Incropera: *Int. J. Heat Mass Transfer*, 1991, vol. 34, pp. 1717-32.
11. T. Fujii, D.R. Poirier, and M.C. Flemings: *Metall. Trans. B*, 1979, vol. 10B, pp. 331-39.
12. M.C. Schneider and C. Beckermann: *Metall. Mater. Trans. A*, 1995, vol. 26A, pp. 2373-88.
13. S.D. Felicelli, D.R. Poirier, A.F. Giamei, and J.C. Heinrich: *JOM*, 1997, vol. 49 (3), pp. 21-25.
14. S.D. Felicelli, D.R. Poirier, and J.C. Heinrich: *J. Cryst. Growth*, 1997, vol. 177, pp. 145-61.
15. M.C. Schneider, J.P. Gu, C. Beckermann, W.J. Boettinger, and U.R. Kattner: *Metall. Mater. Trans. A*, 1997, vol. 28A, pp. 1517-31.
16. M.J.M. Krane and F.P. Incropera: *Int. J. Heat Mass Transfer*, 1997, vol. 40, pp. 3827-35.
17. D.G. Neilson and F.P. Incropera: *Num. Heat Transfer*, 1993, vol. 23, pp. 1-20

18. S.D. Felicelli, J.C. Heinrich, and D.R. Poirier: *J. Cryst. Growth*, 1998, in press.
19. S.D. Felicelli, J.C. Heinrich, and D.R. Poirier: *Int. J. Num. Meth. Fluids*, 1997, vol. 25, pp. 1-21.
20. T.J. Hughes, L.P. Franca, and M. Balestra: *Comp. Meth. Appl. Mech. Eng.*, 1986, vol. 59, pp. 85-99.
21. S.D. Felicelli, P.K. Sung, D.R. Poirier, and J.C. Heinrich: *Int. J. Thermophys.*, 1998, in press.
22. A. Hellawell, J.R. Sarazin, and R.S. Steube: *Phil. Trans. R. Soc. London*, 1993, vol. 345A, pp. 507-44.
23. M.J.M. Krane and F.P. Incropera: *Int. J. Heat Mass Transfer*, 1996, vol. 39, pp. 3567-79.